Indonesian Journal of Electrical Engineering and Computer Science
Vol. 40, No. 3, December 2025, pp. 1270~1284
ISSN: 2502-4752, DOI: 10.11591/ijeecs.v40.i3.pp1270-1284

Optimization of photovoltaic pumping system using neuro fuzzy inference system ANFIS control technique

Laoufi Abdelhaq[1,2,3], Chergui Moulay-Idriss[1], Soufyane Chekroun[1]
[1]Department of Electrical Engineering, Faculty of Sciences and Technology, University Mustapha Stambouli of Mascara, Algeria
[2]Signals and Systems Laboratory, Faculty of Sciences and Technology, University Abdelhamid Ibn Badis of Mostaganem, Algeria
[3]Laboratory of Water Science and Techniques, University of Mascara, Mascara, Algeria

Article Info

Article history:

Received Oct 8, 2024
Revised Oct 27, 2025
Accepted Nov 16, 2025

Keywords:

ANFIS
Direct torque control
Induction motor
MPPT
PV

ABSTRACT

In recent years, artificial intelligence has become increasingly used due to the development of microcontrollers. In this paper, we propose an intelligent technique that employs the adaptive neuro-fuzzy inference system (ANFIS). We use this approach to improve the conventional direct torque control (DTC), which relies on a PI controller for the induction machine, and to enhance the conventional MPPT control based on the Perturb and Observe algorithm. The overall goal is to improve the performance of the photovoltaic pumping system. In this work, we apply ANFIS control to maximum power point tracking (MPPT-ANFIS). Additionally, we simultaneously optimize the efficiency of the DTC by applying ANFIS control (DTC-ANFIS). We present the results by comparing the photovoltaic pumping system using ANFIS control with the conventional photovoltaic pumping system, using MATLAB/Simulink. The results show that ANFIS control significantly improves the photovoltaic system compared to the conventional control, offering excellent dynamic performance of the induction motor and better utilization of photovoltaic solar energy. However, the ANFIS has some drawbacks, such as high computational time consumption and challenges in implementing a database.

Corresponding Author:

Laoufi Abdelhaq
Laboratory of Water Science and Techniques, University of Mascara
BP 763, Mascara 29000, Algeria
Email: abdelhaq.laoufi@univ-mascara.dz

NOMENCLATURE

T_e, T_r : Electromagnetic torque and resistance.
i_{ds}, i_{qs} : Stator currents.
i_{dr}, i_{qr} : Rotor currents.
Φ_{ds}, Φ_{qs} : Stator flux.
Φ_{dr}, Φ_{qr} : Rotor flux.
ω_s : Stator angular electrical speed.
R_s, R_r : Stator and rotor resistances.
L_s,L_r : Stator and rotor inductances.
L_m : Mutual inductance.
p : Number of pole pairs.
J : Moment of inertia.
f : Friction coefficient.
S_a,S_b,S_c : Sequence of the DTC.
E, v_{dc} : The DC voltage of the battery.
V_A,V_B,V_C : Inverter output voltages

1. INTRODUCTION

The pivotal initiation of artificial intelligence (AI) research during the 1950s served as the foundational catalyst for an enduring, sweeping trend toward the diminution of mandatory human effort across all major economic spheres, including industrial manufacturing, modern agricultural processes, and

the expansive service sector [1], [2]. Artificial intelligence fundamentally constitutes a sophisticated, forward-looking analytical technology. Its core strength lies in its ability to meticulously process and interpret extensive volumes of data to produce reliable, well-grounded projections, simultaneously formulating and providing operationally effective and prompt solutions directly extracted from its data-processing outputs. Within control engineering, numerous methodologies exist for intelligent system regulation. In the context of the present investigation, the adaptive neuro-fuzzy inference system (ANFIS) a particularly robust hybrid control methodology will be precisely implemented and evaluated. The central objective of applying ANFIS is the maximization and refinement of the operational effectiveness and performance characteristics of the photovoltaic pumping system [3], [4].

The basis of the ANFIS control is a hybridization of two intelligent controls, fuzzy logic and neural networks. Hybrid neuro-fuzzy networks learn reports and models using a supervised learning algorithm that examines data from a training set consisting of sample inputs and their associated outputs [5]. The ANFIS represents a hybrid architecture that integrates the learning capabilities of an artificial neural network (ANN) with the structured logic of a fuzzy inference system (FIS), leveraging the strengths of each. In an ANFIS framework, the artificial neural network component derives fuzzy rules from the input dataset, while the membership function parameters are adaptively adjusted during the integrated learning procedure. This hybrid system establishes relationships between inputs and outputs through paired input–output data and combines data-driven learning with human expertise [6], [7].

The PV system photovoltaic pumping has different applications. In this work, we focus on of photovoltaic water pumping system. Thanks to its economical price, the induction motor is frequently chosen for use in photovoltaic (PV) water pumping applications, minimal maintenance requirements, and high efficiency. In such systems, the PV module operates near its optimal point, making the additional expense of an inverter relatively insignificant. Recent advancements in efficient inverter technologies for motor speed control have further promoted the use of induction motors in solar pumping applications [8]. The system incorporates a centrifugal pump, which is actuated by a three-phase asynchronous motor [8].

The technique of direct torque control (DTC), which invented by TAKAHASHI In 1985, it use an attractive approach due to its efficiency and simplicity of implementation [9]. Several works allow a rigorous modeling of this approach [10]. This technique makes it possible to calculate the control quantities, which are the stator flux and the electromagnetic torque from the measurements of the stator currents without using a mechanical sensor. In the DTC structure [11], [12]. In DTC, the appropriate voltage vector is directly selected from a predefined switching table according to the DTC principle to regulate the converter operation. This approach enables the system to achieve a fast dynamic torque response. The torque and stator flux errors are maintained within a specified band using hysteresis controllers; however, this method inherently produces significant torque ripple [13], [14].

2. MÉTHODE

2.1. Hardware modeling

2.1.1. Stat representation of IM in Parck's reference system

In order to control and observe the behaviour of the asynchronous machine, a state representation is required. To accomplish this objective, we have considered the state vector, which is consisting of the stator currents, and the rotor fluxes.

The full mathematical representation of the asynchronous machine, derived from the work of [15], is presented below:

$$\begin{cases} \frac{dI_{ds}}{dt} = \frac{1}{\sigma L_s}\left[-(R_s + (\frac{L_m}{L_r})^2 R_r)I_{ds} + \sigma L_s \omega_s I_{qs} + \frac{L_m R_r}{{L_r}^2}\Phi_{dr} + \frac{L_m}{L_r}\Phi_{qr}\omega + V_{ds}\right] \\ \frac{dI_{qs}}{dt} = \frac{1}{\sigma L_s}\left[-\sigma L_s \omega_s I_{ds} - (R_s + (\frac{L_m}{L_r})^2 R_r)I_{qs} - \frac{L_m}{L_r}\Phi_{dr}\omega + \frac{L_m R_r}{{L_r}^2}\Phi_{qr} + V_{qs}\right] \\ \frac{d\Phi_{dr}}{dt} = -\frac{L_m R_r}{L_r} I_{ds} - \frac{R_r}{L_r}\Phi_{dr} + (\omega_s - \omega)\Phi_{qr} \\ \frac{d\Phi_{qr}}{dt} = -\frac{L_m R_r}{L_r} I_{qs} - \frac{R_r}{L_r}\Phi_{qr} - (\omega_s - \omega)\Phi_{dr} \\ \frac{d\omega}{dt} = \frac{p^2 L_m}{L_r J}(\Phi_{dr} I_{qs} - \Phi_{qr} I_{ds}) - \frac{f}{J}\omega - \frac{P}{J}C_r \end{cases} \quad (1)$$

Where $\sigma$the coefficient of dispersion is $\sigma = 1 - \frac{{L_m}^2}{L_s L_r}$.

2.1.2. Centrifugal pump modelling

In PV water pumping systems, the hydraulic pump plays a crucial role. The centrifugal pump is the most commonly employed type due to its simple operation and modular design flexibility. Based on the principles of the Bernoulli equation, the rotodynamic pump converts the electrical power delivered by its drive unit into the kinetic energy of the working fluid by accelerating the fluid's rotation [16]. The corresponding pump characteristic curve defines the correlation connecting the volumetric flow and the net differential head at a fixed rotational speed, which may be approximated as [16], [17]:

$$H_{pump} = a_0 + a_1 Q + a_2 Q^2 \quad (2)$$

$$H_{pipline} = H_g + \Delta H \quad (3)$$

$$\frac{Q}{Q_0} = \frac{w}{w_0}; \frac{H}{H_0} = \left(\frac{w}{w_0}\right)^2; \frac{T}{T_0} = \left(\frac{w}{w_0}\right)^2; \frac{P}{P_0} = \left(\frac{w}{w_0}\right)^3 \quad (4)$$

a_0, a_1, a_2: Are the specific constants defining the pump's performance
Q, H: Are defined as the pump's discharge head and flow capacity, respectively
H_g: Is the geometric level of the system
ΔH: Represents the total head loss attributable to friction and local resistance within the pipeline.

Typically, hydraulic pump manufacturers provide only the nominal performance characteristics corresponding to the rated operating speed w_0, which are respectively, frequency T_0, power P_0, flow rate Q_0 and the head H_0 [17].

2.1.3. Modeling the two-level voltage source inverter

A static DC/AC power electronic converter, a three-phase inverter is configured to generate three balanced output voltages, allowing for precise adjustment of both their magnitude and frequency. The converter's operation is effectively modeled as a conventional two-level voltage source inverter (VSI-2L) for simulation purposes. Figure 1 presents the equivalent schematic of the VSI-2L, which draws its power from a continuous DC supply specifically, a PV panel in this application. This DC/AC converter then acts as the electrical energy source for the induction machine [18].

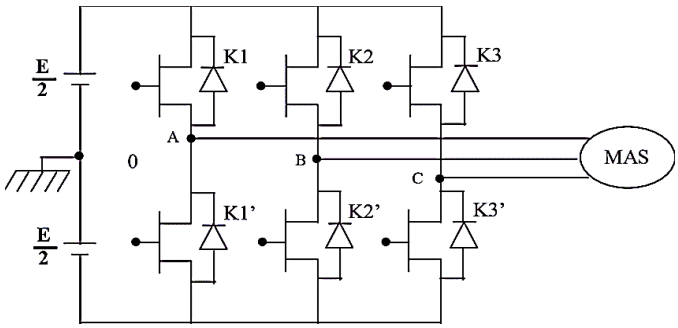

Figure 1. Voltage source inverter

The following section details the mathematical model for the two-level voltage inverter, as established by [17]:

$$\begin{bmatrix} V_{An} \\ V_{Bn} \\ V_{Cn} \end{bmatrix} = \frac{E}{3} \begin{vmatrix} 2 & -1 & -1 \\ -1 & 2 & -1 \\ -1 & -1 & 2 \end{vmatrix} \begin{vmatrix} S_a \\ S_b \\ S_c \end{vmatrix} \quad (5)$$

2.1.4. PV array modelling

The mathematical representation of a PV module begins with the single-diode model for a PV cell. This electrical analog is comprised of a current generator (I_{pv}), an inversely connected diode (D), a series resistance (R_s), and a shunt resistance (R_p), as depicted in Figure 2 [18].

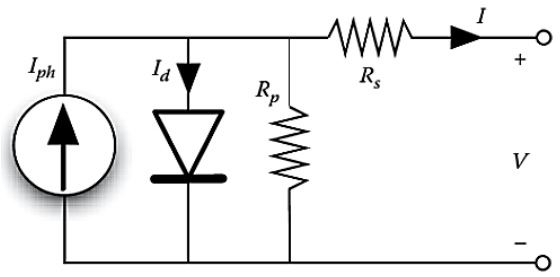

Figure 2. Equivalent circuit of photovoltaic cell

The output current of the PV cell represented by the following expression:

$$I = I_{pv} - I_s\left\{exp\left(\frac{q}{AKT_sN_s}V + IR_s\right) - 1\right\} - \frac{V+IR_s}{R_p} \quad (6)$$

where:
I_s: The reverse saturation current of the photovoltaic cell
A: The diode ideality factor of the joint
q: Electron charge
K: Boltzmann constant
N_s: The number of series connected cells
The light generated current (I_{pv}) in (7) expressed as:

$$I_{pv} = \left[I_{sc} + K_1\left(T_c - T_{ref}\right)\right]G \quad (7)$$

where:
K_1: The thermal coefficient associated with the cell's short-circuit current
T_{ref},T_c: Correspond to the operating and reference temperatures of the cell, respectively
G: Corresponds to the level of solar irradiance, given in w/m^2
The saturation current of the photovoltaic cell's diode, denoted as (I_s) is defined as:

$$I_s = I_{RC}\left(\frac{T_c}{T_{ref}}\right)^3 exp\left[\frac{qE_g}{A_k}\left(\frac{1}{T_c} - \frac{1}{T_{ref}}\right)\right] \quad (8)$$

The reverse saturation current is:

$$I_{RS} = \frac{I_{SC}}{exp\left(\frac{q}{AKT_cN_S}V_{oc}\right)-1} \quad (9)$$

To reduce the number of PV panels required, a boost converter is employed to increase the output voltage of the DC source. The circuit diagram of the boost converter is presented in Figure 3 [19].

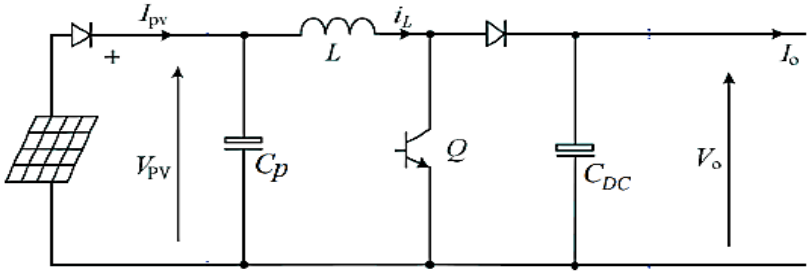

Figure 3. Boost converter circuit

2.2. Technical control system

2.2.1. The direct torque control

Based on the decoupled control of electromagnetic torque and stator flux linkage, the fundamental principle of DTC involves the direct selection of stator voltage vectors. The control mechanism is realized by instantaneously varying the stator voltage vectors in response to the errors observed in the torque and stator flux [18], [19].

Figure 4 shows a diagram summarizing the general principle of the DTC technique. Currents I_a, I_b, I_c and voltages V_a, V_b, V_c are measured at the output of the inverter, and after passing through the park transformation we obtain currents $I_d, I_q$and voltages V_d, V_q, which are used to estimate the electromagnetic torque and flux in the relationships (10), (11). The estimated torque and flux will compared with the reference torque and flux, and the results of the comparison are the inputs of the hysteresis controllers, which will give the output either 1,-1 or 0. The switching states for the voltage source inverter are determined by a selected voltage vector, which is then decomposed and used to apply the correct switching table, as shown in Table 1 [20], [21].

$$\begin{cases} \varphi_{\alpha\, s} = \int_0^t (V_{\alpha_s} - R_s\, I_{\alpha_s})dt \\ \varphi_{\beta\, s} = \int_0^t (V_{\beta_s} - R_s\, I_{\beta_s})dt \end{cases} \tag{10}$$

$$C_{em} = p(\varphi_{\alpha_s}\, I_{\beta_s} - \varphi_{\beta_s}\, I_{\alpha_s}) \tag{11}$$

Table 1. The takahashi vector selection chart

N		1	2	3	4	5	6
$\boldsymbol{H_{Te}=1}$	$H_\varphi = 1$	V_2	V_3	V_4	V_5	V_6	V_1
	$H_\varphi = 0$	V_7	V_0	V_7	V_0	V_7	V_7
	$H_\varphi = -1$	V_6	V_1	V_2	V_3	V_4	V_5
$\boldsymbol{H_{Te}=0}$	$H_\varphi = 1$	V_3	V_4	V_5	V_6	V_1	V_2
	$H_\varphi = 0$	V_0	V_7	V_0	V_7	V_0	V_7
	$H_\varphi = -1$	V_5	V_6	V_1	V_2	V_3	V_4

To control speed, we integrate a PI controller, which uses at its input the variation between the set speed and the measured speed, which will define at its output the reference torque. The relationship (12) presents the transfer function of the PI controller [14], [19].

$$C_{ref} = k_p e_s(t) + k_i \int e_s(t)dt \tag{12}$$

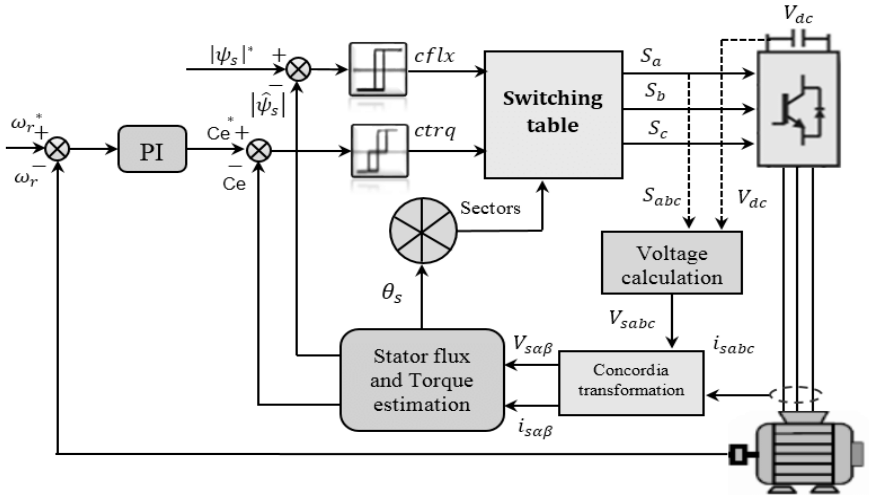

Figure 4. Block diagram of DTC-PI applied on induction machine

2.2.2. MPPT technique

Due to the non-linearity of PV power and voltage variation, solar power systems need to maximum power point tracking (MPPT) control, which depends on photovoltaic insolation and temperature, With the objective of operating photovoltaic modules at maximum power points to produce maximum power with the use of less expensive and more efficient equipment [22], [23]. There are a number of conventional algorithms, such as perturbation and P&O observation [24]. Figure 5 presents the disturbance and observation algorithm applied to the photovoltaic panel.

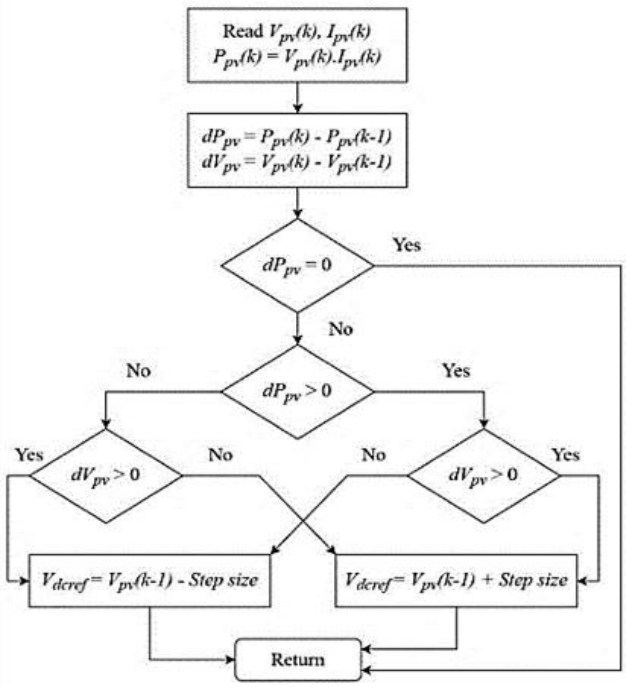

Figure 5. Flowchart of the conventional perturb and observe algorithm [25]

2.2.3. Adaptive neuro-fuzzy inferencing systems

Computational intelligence techniques such as artificial neural networks (ANN), fuzzy systems, and ANFIS are well-suited for modeling and control of nonlinear systems. ANFIS operates as a hybrid controller that integrates the advantages of both fuzzy logic control (FLC) and neural networks (NN) [26]. In this approach, neural networks are employed to generate fuzzy membership functions and construct the rule base through a supervised training process [27]. Two fuzzy if–then rules are considered in the ANFIS structure, as illustrated in Figure 6 [24], [28].

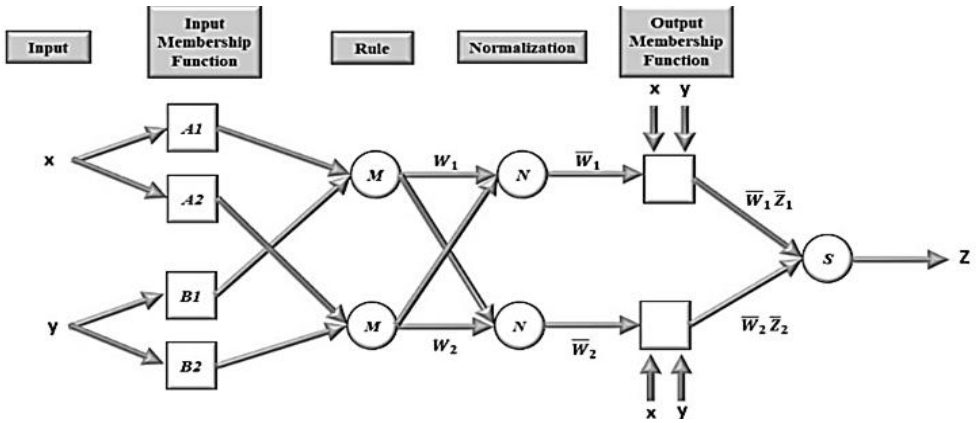

Figure 6. Global architecture for Neuro-Fuzzy ANFIS [28]

The ANFIS architecture is composed of five distinct layers. Within the model's antecedent, Ai and Bi represent the fuzzy sets. Concurrently pi, qi, and ri function as the design parameters whose values are determined during the training phase [29]. The first of the five structural elements is designated as the fuzzification layer. The output generated by the node in this initial layer is expressed using the subsequent [30], [31]:

$$O_i^1, i = \mu_{Ai}(x) = exp\left\{-\left[\left(\frac{x-c_i}{\sigma_i}\right)^2\right]\right\}, where, i = 1,2 or O_1, i = \mu_{Bi}(y), i = 3,4, \quad (13)$$

x=node input, {σi, bi, ci} =starting parameter
If μ_{Ai} and μ_{Bi} are Gaussian MFs, they are specified by two parameters {c, σ}.
Layer 2: Each node determines the firing strength of a rule, and the output of node i is expressed by the following [32]:

$$O_i^2 = w_i = \mu_{Ai}(x_1).\mu_{Bi}(x_2).i = 1,2 \quad (14)$$

Layer 3: The nodes normalize the firing strengths of the rules, and the output of node i is given by the following [33]:

$$\overline{w_i} = \frac{w_i}{\sum_{k=1}^{n} w_k} \quad (15)$$

Layer 4: This layer performs the defuzzification and produces the final results. The weighted consequent values for each rule are computed at every node within this layer, using (16) for their calculation [34].

$$O_{4i} = \overline{w_i} f_i = \overline{w_i}(p_i x + q_i y + r_i) \quad (16)$$

To optimize the parameters of ANFIS, both least squares estimation and back-propagation methods adopted. Figure 7 shows the explanatory diagram of neural networks. Figures 7(a) represents the result of training stage is five Gaussian membership functions for DTC-ANFIS, and Figures 7(b) represents the result of training stage is three Gaussian membership functions for MPPT-ANFIS [34], [35].

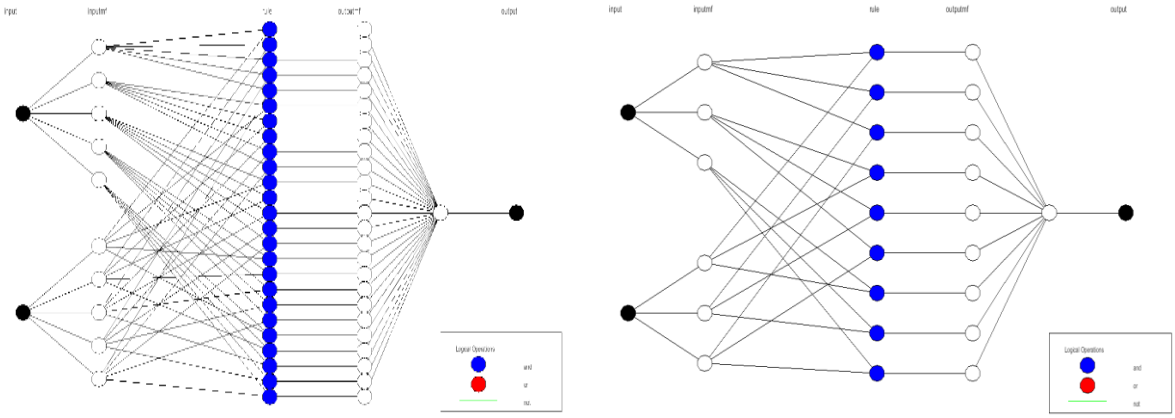

(a) (b)

Figure 7. Network structure for (a) DTC-ANFIS and (b) MPPT-ANFIS

As depicted in Figure 8, the photovoltaic water pumping system is usually structured around two primary subsystems:

– The power circuit, which includes the solar panels, a parallel (boost) converter, a two-level inverter, an asynchronous motor coupled to acentrifugal pump.

– The control circuit, which integrates: An MPPT-ANFIS controller applied to the boost converter to optimize maximum power extraction from the solar panels. a DTC-ANFIS controller applied to the inverter to ensure DTC of the motor.

The boost converter is directly powered by the solar panels and, thanks to the MPPT-ANFIS control, delivers an optimal DC voltage to the inverter. The two-level inverter then converts this voltage into a three-phase sinusoidal AC voltage to drive the induction motor. The inverter receives its switching signals from the DTC-ANFIS controller, which provides accurate torque control. The motor then drives the centrifugal pump, enabling water to be pumped into a well or a storage tank.

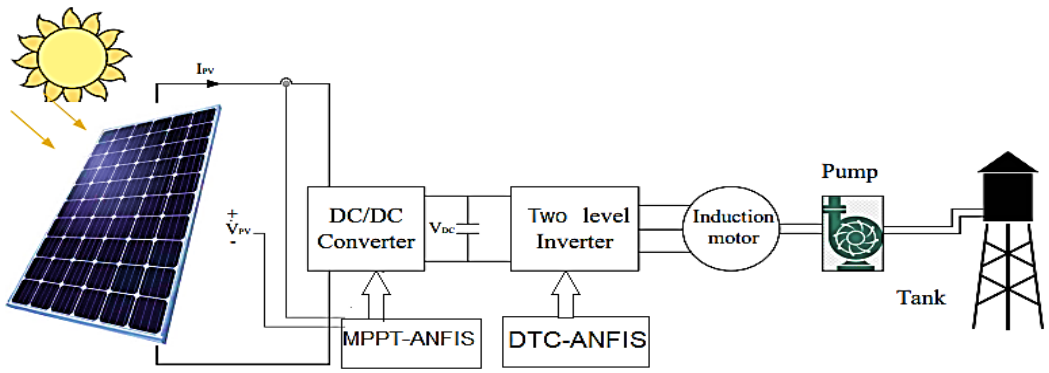

Figure 8. Block diagram of the ANFIS-based control applied to a photovoltaic pumping system [36]

2. RESULTS AND DISCUSSION

To gain a deep and precise understanding of the dynamic characteristics of the photovoltaic water pumping system, its target circuit was meticulously replicated within the MATLAB/Simulink simulation environment. This comprehensive simulation was designed to explore how the system's performance evolves over time, particularly under fluctuating operational conditions. For manageability and clarity, the overall model has been systematically organized into a modular framework consisting of five primary functional blocks. This architectural breakdown is visually represented and detailed for reference in Figure 9, outlining the key components and their interconnections.

– DC Power Supply Block: This subsystem includes the photovoltaic panels, connected to a Boost converter (parallel chopper) controlled by an MPPT-ANFIS controller. The controller dynamically adjusts the operating point of the PV generator based on solar irradiance and ambient temperature, in order to provide a stable and optimal DC voltage to the inverter input.
– DTC-ANFIS Control Block: This block implements a DTC strategy enhanced by an ANFIS. It generates in real-time the switching signals (Sa, Sb, Sc) for the inverter, ensuring fast and robust regulation of the motor's torque and stator flux.
– Two-Level Inverter Block: This static converter receives both the DC voltage from the MPPT block and the modulation signals from the DTC-ANFIS controller. It converts the DC power into a three-phase sinusoidal AC voltage suitable for driving the induction motor.
– Induction Motor Block: This block simulates the electromechanical behavior of the asynchronous machine. It is powered by the inverter and subjected to a variable load torque imposed by the centrifugal pump. The dynamic equations account for the electromagnetic interactions between the stator and rotor.
– The Centrifugal Pump Block represents and simulates the entire hydraulic load which the induction motor directly drives and mechanically couples to the machine's shaft. This crucial modeling component receives the measured rotor speed from the motor as its sole input signal. In direct response to this rotation, the block then calculates and produces a specific resistant torque. This resistant torque effectively opposes the motor's motion, accurately reflecting the mechanical demand that the pump places on the motor drive system as it works to move the fluid.

This section is dedicated to the rigorous validation of the proposed system through a series of simulations meticulously executed within the MATLAB/Simulink environment. To accurately construct and configure the computational models necessary for these tests, we have relied upon two critical sets of specifications. Specifically, the dynamic behavior of the motor components is modeled using the detailed induction motor parameters comprehensively enumerated in Table 2, while the power generation

characteristics are defined by the specific photovoltaic (PV) panel specifications as outlined in Table 3. These simulation runs are intentionally conducted under standardized, repeatable operating conditions to ensure consistent and comparable results. These controlled environmental inputs are set at an ambient temperature of 22°C and a peak solar irradiance level of $1000\text{ W}/\text{m}^{2}$. This defined environment allows for a clear assessment of the system's performance before considering more variable real-world conditions.

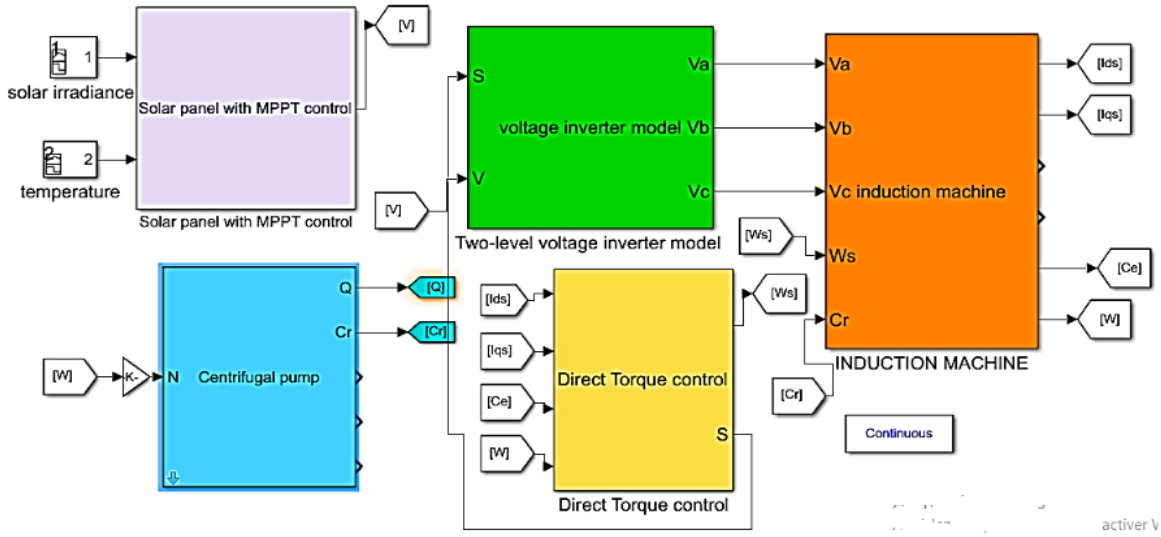

Figure 9. Global block diagram of the neuro-fuzzy control applied to a photovoltaic pumping system in MATLAB/Simulink

Table 2. Characteristics of the induction machine

Greatness	Value	Greatness	Value
Rated power	1.5kw	Rotor resistance	3.805Ω
Rated voltage	220V	Cyclic stator inductance	0.274H
Rated speed	1428rpm	Cyclic rotor inductance	0.274H
Nominal frequency	50Hz	Mutual inductance	0.258H
Rated stator current	3.64A	Number of pole pairs	2
Stator resistance	4.85 Ω	Moment of inertia	0.031kg/m2
Friction coefficients	0.00114Nm.s/rd		

Table 3. Characteristics of photovoltaic panel

Greatness	Value
Maximum Power (W)	213W
Open circuit voltage	36.3V
Voltage at maximum power point	29V
Cells permodule	60
Short-circuit current	7.84A
Current at maximum power point Imp	7.35A

Figure 10 shows the MPPT control results by displaying the evolution of the photovoltaic voltage. It compares two control strategies: the ANFIS-based MPPT control, represented by the solid red line, and the conventional P&O-based MPPT control, represented by the dashed blue line. The analysis highlights that the MPPT-ANFIS approach tracks the maximum power point (MPP) more quickly and accurately, significantly reducing steady-state oscillations compared to the P&O method. This improvement enhances both the system's stability and energy conversion efficiency.

Figure 11 shows the MPPT control results by displaying the evolution of the photovoltaic power. It compares two control strategies: the ANFIS-based MPPT control, represented by the solid red line, and the conventional P&O-based MPPT control, represented by the dashed blue line. The observation confirms that the ANFIS-based control extracts energy more efficiently by ensuring more accurate and stable MPP

tracking. Additionally, it improves power quality by reducing oscillations and delivering a faster, more responsive dynamic behavior than the P&O strategy.

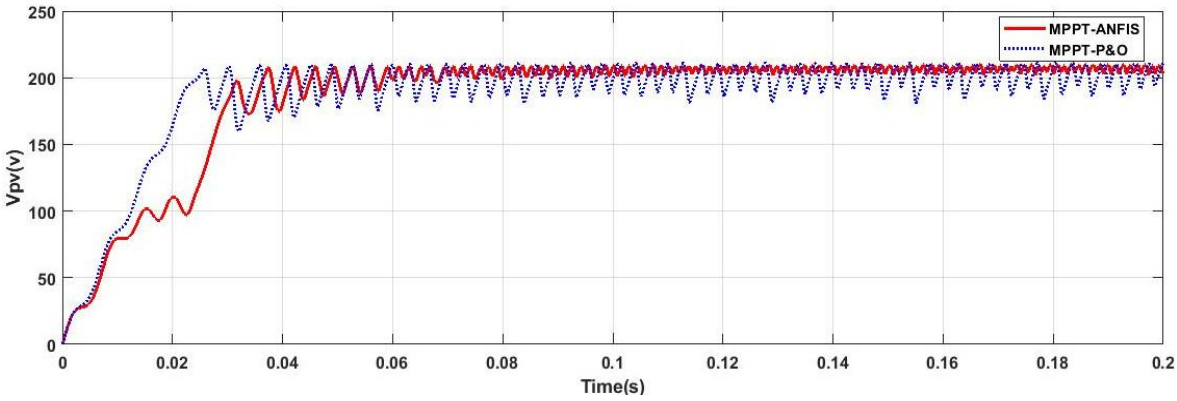

Figure 10. The voltage delivered by the photovoltaic panel

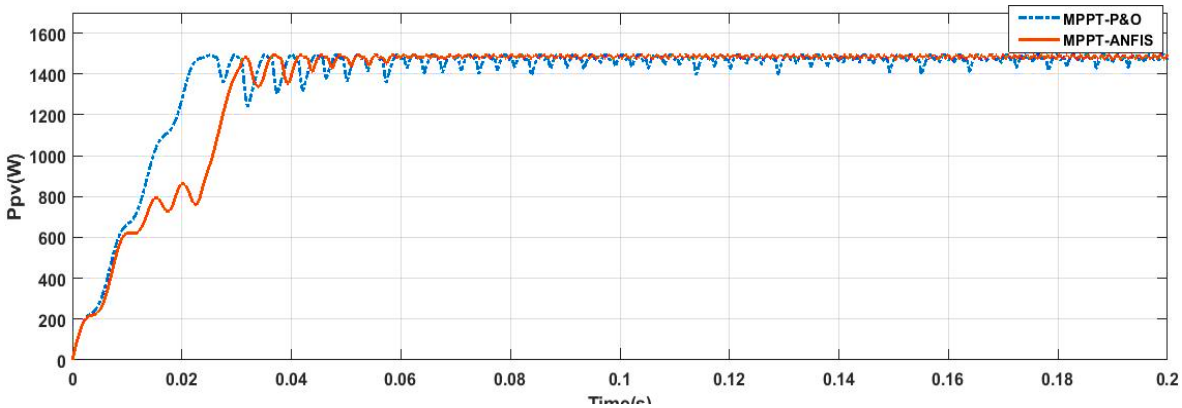

Figure 11. The generated power of the photovoltaic module

This analytical section examines and dissects the behavior of the machine's primary dynamic quantities, specifically focusing on the rotor speed, the developed electromagnetic torque, and the instantaneous stator current. We compare the performance achieved by the two tested control strategies: the intelligent DTC with adaptive neuro-fuzzy inference system (DTC-ANFIS, which the solid red curve represents), and the conventional DTC with Proportional-Integral regulator (DTC-PI, which the dashed blue curve represents). Beyond the electrical and mechanical aspects, this analysis presents the evolution of the hydraulic flow rate that the centrifugal pump generates. This comprehensive evaluation ultimately demonstrates how the intelligent ANFIS control significantly improves the overall operational performance of the photovoltaic pumping system when benchmarked against the limitations of the traditional PI-based control scheme.

Figure 12 shows the dynamic response of the rotor speed. Between 0 s and 0.03 s, the system exhibits an initial delay, mainly due to the transient behavior of the DC voltage generated by the photovoltaic panels, which determines the inverter’s power supply. In steady state, the intelligent control strategy based on the ANFIS algorithm reaches a stable rotor speed of 148 rad/s with a response time of 0.19 s. In comparison, the conventional control using a PI regulator reaches a maximum speed of only 144 rad/s, with a response time of 0.17 s. This limitation results from the resistive torque caused by the pump's loaded startup. Although both methods offer similar response times, the 4 rad/s difference in steady-state speed directly impacts the hydraulic flow rate, which is proportional to the motor shaft speed. Therefore, the ANFIS-based control stands out for its better adaptability to load variations, more efficient use of the available solar energy, and a significant improvement in the overall efficiency of the pumping system.

Figure 13 illustrates the evolution of the electromagnetic torque for both control strategies. During the startup phase, both controllers produce an initial torque of approximately 40 Nm to overcome the resistive torque generated by the loaded startup of the centrifugal pump. Under steady-state conditions, the electromagnetic torque stabilizes at around 6.3 Nm, which compensates for fluctuations in the load torque and ensures a constant rotor speed.

However, a comparative analysis reveals that the conventional control strategy, based on the PI controller and the P&O algorithm produces more pronounced harmonics in the torque profile, as shown in Figure 14. These fluctuations indicate a less consistent response and may lead to undesirable mechanical vibrations within the machine. In contrast, the ANFIS-based control yields fewer harmonics compared to conventional control, thereby reducing mechanical disturbances, improving user comfort, and extending the lifespan of the system's electromechanical components.

Figure 15 visually details how the stator current evolves across the simulation time frame. The two distinct control strategies—the standard DTC-PI and the advanced DTC-ANFIS—each generate a noticeable transient response in the current signal. Crucially, the DTC-ANFIS control draws a measurably higher current during this transient period compared to the current the DTC-PI control utilizes. While both signals contain similar harmonic profiles, the difference in the controllers' time responses ultimately causes a minor, yet detectable, phase shift between the two current waveforms.

Figure 16 offers a direct comparison, illustrating how the two distinct regulation strategies generate the hydraulic flow rates throughout the operational cycle. During the initial system startup, both controllers exhibit a necessary delay before achieving significant fluid movement. The conventional control incurs a startup lag of 0.14s, while the intelligent ANFIS control shows a slightly longer initial delay, which reaches 0.15 s. This phenomenon occurs because the pumping system must first reach a specific rotational speed threshold; only then can it produce the necessary head to establish an increased flow rate. Once the system transitions into steady-state conditions, the ANFIS controller clearly outperforms its counterpart. The ANFIS controller produces and maintains a highly stable flow rate of 1.8L/s, a performance level that significantly exceeds the 1.6L/s flow rate which the conventional regulation strategy provides. This stable, higher output demonstrates the superior efficiency of the ANFIS approach in sustained operation.

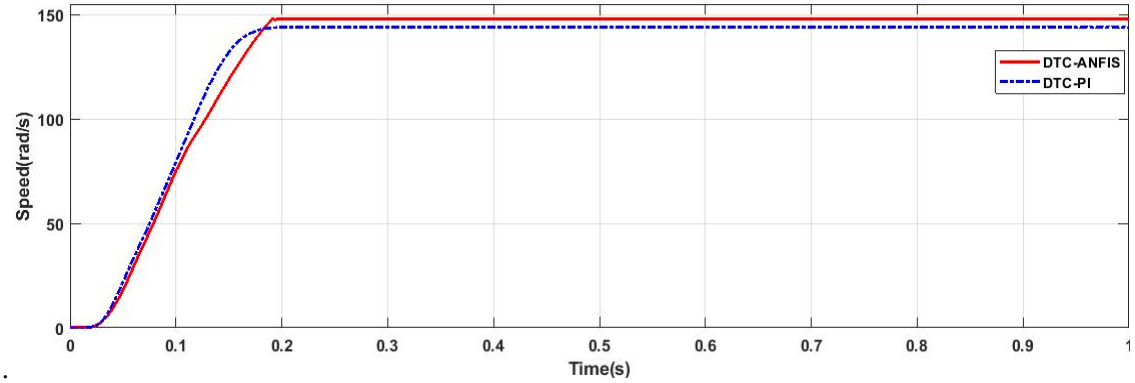

Figure 12. Comparison of induction motor speed responses using DTC-PI and DTC-ANFIS techniques

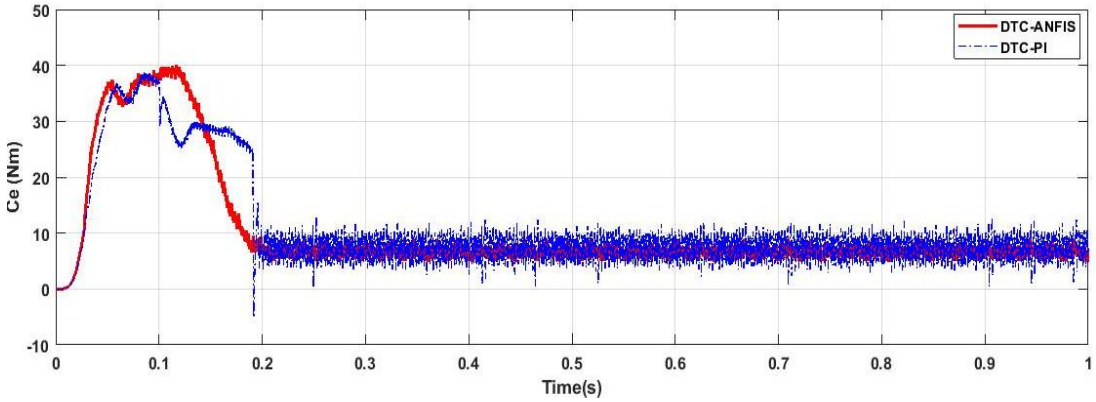

Figure 13. Comparison of torque responses using DTC-PI and DTC-ANFIS techniques

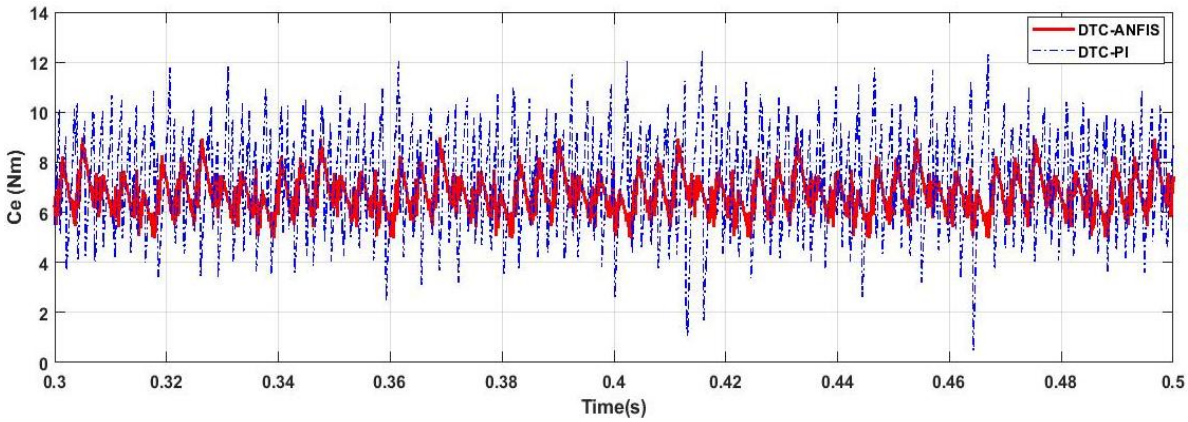

Figure 14. Detailed view of torque responses

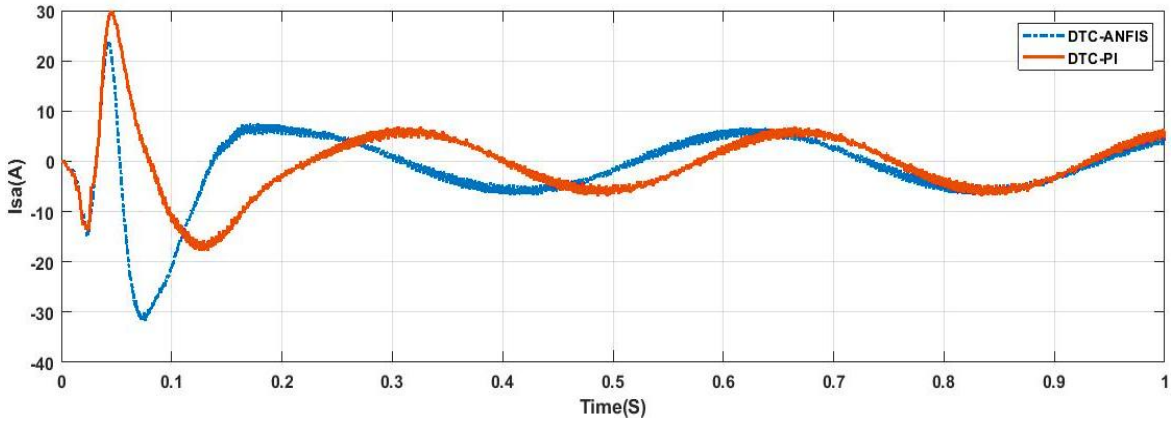

Figure 15. Comparison of stator current using DTC-PI and DTC-ANFIS techniques

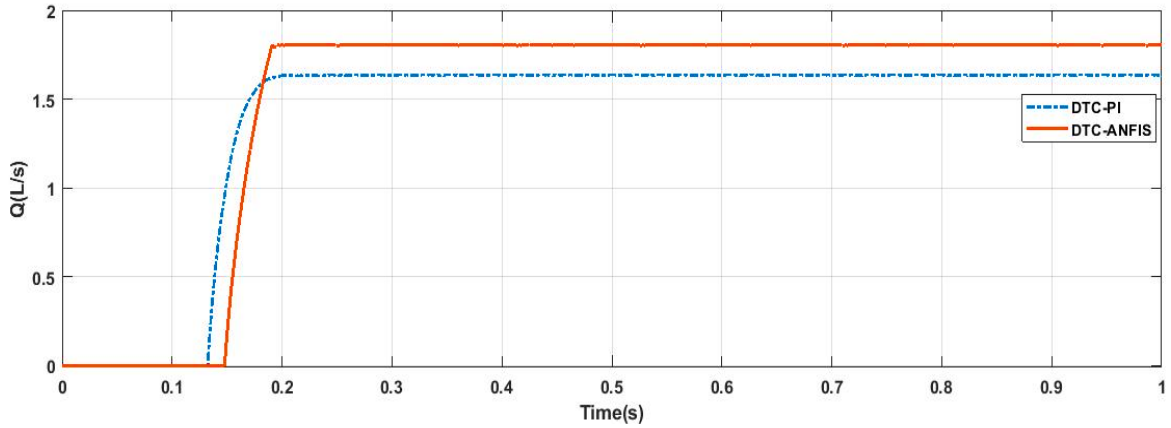

Figure 16. Comparison of the hydraulic flow rates DTC-PI and DTC-ANFIS techniques

This marked improvement in system output originates directly from the superior dynamic performance inherent to the ANFIS control system. As previously established, this intelligent controller excels at maintaining a higher and notably more stable rotor speed while concurrently achieving a crucial reduction in electromagnetic torque oscillations. Given that the flow rate of a centrifugal pump is inherently and directly proportional to its shaft rotational speed, this distinct operational advantage immediately translates into a more optimal and efficient utilization of the available hydraulic power. Consequently, the ANFIS control methodology decisively proves to be significantly more effective at maximizing the transfer

of energy—from the intermittent photovoltaic source directly into the hydraulic load. The end result of this optimized control loop is a substantial enhancement in the overall energy efficiency and performance capacity of the entire photovoltaic pumping system.

3. CONCLUSION

This work focused on optimizing a photovoltaic water pumping system by integrating an intelligent control strategy based on the ANFIS. We compared this approach with conventional methods that combine a PI controller and the Perturb and Observe (P&O) algorithm. We applied the ANFIS controller to both DTC and MPPT. The simulations performed in MATLAB/Simulink showed that the ANFIS-based controller effectively tracked the maximum power point and significantly improved the quality of the energy extracted through MPPT. On the machine side, it delivered a clearly superior dynamic response: it maintained a higher and more stable rotor speed, reduced torque harmonics and ripple, and achieved a higher hydraulic flow rate compared to the conventional controller. These improvements helped reduce mechanical vibrations, extend motor lifespan, and enhance the overall utilization of the available hydraulic power.

ACKNOWLEDGEMENTS

The authors would like to express their sincere gratitude to the Algerian Ministry of Higher Education and Scientific Research for its support and encouragement of academic research.

FUNDING INFORMATION

The authors state that this work was funded by the Mustapha Stambouli University of Mascara, Algeria.

AUTHOR CONTRIBUTIONS STATEMENT

This journal uses the Contributor Roles Taxonomy (CRediT) to recognize individual author contributions, reduce authorship disputes, and facilitate collaboration.

Name of Author	C	M	So	Va	Fo	I	R	D	O	E	Vi	Su	P	Fu
Laoufi Abdelhaq	✓	✓	✓	✓	✓	✓	✓	✓	✓	✓				
Chergui Moulay-Idriss		✓		✓	✓	✓				✓	✓	✓		
Soufiane Chekroun		✓		✓	✓					✓	✓	✓		

C : **C**onceptualization
M : **M**ethodology
So : **So**ftware
Va : **Va**lidation
Fo : **Fo**rmal analysis
I : **I**nvestigation
R : **R**esources
D : **D**ata Curation
O : Writing - **O**riginal Draft
E : Writing - Review & **E**diting
Vi : **Vi**sualization
Su : **Su**pervision
P : **P**roject administration
Fu : **Fu**nding acquisition

CONFLICT OF INTEREST STATEMENT

Authors state no conflict of interest.

DATA AVAILABILITY

Derived data supporting the findings of this study are available from the corresponding author, [LA], on request.

REFERENCES

[1] I. Akkurt, P. B. Malidarreh, and R. Boodaghi Malidarre, "Simulation and prediction of the attenuation behaviour of the KNN–LMN–based lead-free ceramics by FLUKA code and artificial neural network (ANN)–based algorithm," *Environmental Technology*, vol. 44, no. 11, pp. 1592–1599, May 2023, doi: 10.1080/09593330.2021.2008017.

[2] M. T. Çelik and S. Arslankaya, "Analysis of quality control criteria in a business with the fuzzy DEMATEL method: Glass business example," *Journal of Engineering Research*, vol. 11, no. 2, p. 100039, Jun. 2023, doi: 10.1016/j.jer.2023.100039.

[3] R. B. Malidarre, I. Akkurt, P. B. Malidarreh, and S. Arslankaya, "Investigation and ANN-based prediction of the radiation shielding, structural and mechanical properties of the Hydroxyapatite (HAP) bio-composite as artificial bone," *Radiation Physics and Chemistry*, vol. 197, p. 110208, Aug. 2022, doi: 10.1016/j.radphyschem.2022.110208.
[4] Y. Lahiouel, S. Latreche, and M. Khemliche, "ANFIS based method for faults detection in the photovoltaic system," *Indonesian Journal of Electrical Engineering and Computer Science*, vol. 32, no. 2, p. 773–786, Nov. 2023, doi: 10.11591/ijeecs.v32.i2.pp773-786.
[5] R. Belal, M. Flitti, and M. L. Zegai, "Tuning of PI speed controller in direct torque control of dual star induction motor based on genetic algorithms and neuro-fuzzy schemes," *Revue Roumaine des Sciences Techniques – Série Électrotechnique et Énergétique*, vol. 69, no. 1, pp. 9–14, Apr. 2024, doi: 10.59277/RRST-EE.2024.1.2.
[6] I. P. Okokpujie and J. E. Sinebe, "An overview of the study of ANN-GA, ANN-PSO, ANFIS-GA, ANFIS-PSO and ANFIS-FCM predictions analysis on tool wear during machining process," *Journal Européen des Systèmes Automatisés*, vol. 56, no. 2, pp. 269–280, Apr. 2023, doi: 10.18280/jesa.560212.
[7] J. Dou, C. Xu, S. Jiao, B. Li, J. Zhang, and X. Xu, "An unsupervised online monitoring method for tool wear using a sparse auto-encoder," *International Journal of Advanced Manufacturing Technology*, vol. 106, no. 5–6, pp. 2493–2507, Jan. 2020, doi: 10.1007/s00170-019-04788-7.
[8] D. S. Sawant, Y. Srinivasa Rao, and R. R. Sawant, "A hybrid combination of improved mayfly optimization-based modified perturb and observe for solar-based water pumping system," *Indonesian Journal of Electrical Engineering and Computer Science*, vol. 38, no. 1, pp. 50–62, Apr. 2025, doi: 10.11591/ijeecs.v38.i1.pp50-62.
[9] N. El Ouanjli *et al.*, "Modern improvement techniques of direct torque control for induction motor drives—A review," *Protection and Control of Modern Power Systems*, vol. 4, no. 1, p. 11, Dec. 2019, doi: 10.1186/s41601-019-0125-5.
[10] N. Priyadarshi, S. Padmanaban, J. B. Holm-Nielsen, V. K. Ramachandaramurthy, and M. S. Bhaskar, "An adaptive neuro-fuzzy inference system employed Cuk converter for PV applications," in *Proc. IEEE 13th Int. Conf. Compatibility, Power Electronics and Power Engineering (CPE-POWERENG)*, Sonderborg, Denmark, Apr. 2019, pp. 1–5, doi: 10.1109/CPE.2019.8862398.
[11] S. Ambarapu *et al.*, "Analysis of fuzzy and neural controllers in direct torque controlled synchronous motors," *Indonesian Journal of Electrical Engineering and Computer Science*, vol. 32, no. 2, pp. 676–687, Nov. 2023, doi: 10.11591/ijeecs.v32.i2.pp676-687.
[12] S. A. B. Ahmad Tarusan, A. Jidin, and M. L. M. Jamil, "The simulation analysis of torque ripple reduction by using optimal voltage vector in DTC fed by five-level CHB inverter," *Indonesian Journal of Electrical Engineering and Computer Science*, vol. 20, no. 3, pp. 1665–1676, Dec. 2020, doi: 10.11591/ijeecs.v20.i3.pp1665-1676.
[13] N. H. Viet and P. D. Dai, "A comparison of DTC and PTC techniques for induction motor drive systems," in *Proc. 2021 13th Int. Conf. Electronics, Computers and Artificial Intelligence (ECAI)*, Pitesti, Romania, Jul. 2021, pp. 1–5, doi: 10.1109/ECAI52376.2021.9515130.
[14] H. Zekraoui, T. Ouchbel, and M. L. El Hafyani, "Comparative study of wind turbine emulator control using an asynchronous motor: IRFOC and DTC," *Indonesian Journal of Electrical Engineering and Computer Science*, vol. 36, no. 1, pp. 174–187, Oct. 2024, doi: 10.11591/ijeecs.v36.i1.pp174-187.
[15] M. Aktas, K. Awaili, M. Ehsani, and A. Arisoy, "Direct torque control versus indirect field-oriented control of induction motors for electric vehicle applications," *Engineering Science and Technology, an International Journal*, vol. 23, no. 5, pp. 1134–1143, Oct. 2020, doi: 10.1016/j.jestch.2020.04.002.
[16] T. Ouchbel *et al.*, "Power maximization of an asynchronous wind turbine with a variable speed feeding a centrifugal pump," *Energy Conversion and Management*, vol. 78, pp. 976–984, Feb. 2014, doi: 10.1016/j.enconman.2013.08.063.
[17] S. Philippe Barret, "Régimes transitoires des machines tournantes électriques," in *Direction des Études et Recherches d'Électricité de France (EDF), Cours de l'École Supérieure d'Électricité*, 1987, p. 216.
[18] D. Casadei, G. Serra, A. Tani, and L. Zarri, "Direct torque control for induction machines: A technology status review," in *Proc. IEEE Workshop on Electrical Machines Design, Control and Diagnosis (WEMDCD)*, Paris, France, Mar. 2013, pp. 117–129, doi: 10.1109/WEMDCD.2013.6525172.
[19] M. S. Kumar, G. Satheesh, and S. Peddakotla, "Design of optimal PI controller for torque ripple minimization of SVPWM-DTC of BLDC motor," *International Journal of Power Electronics and Drive Systems*, vol. 14, no. 1, pp. 283–293, Mar. 2023, doi: 10.11591/ijpeds.v14.i1.pp283-293.
[20] M. Dybkowski, "Induction motor stator faults identification using modified MRAS type estimator," *Electrotechnical Review*, vol. 1, no. 5, pp. 216–221, May 2023, doi: 10.15199/48.2023.05.37.
[21] A. Ahmed, "Real time implementation of fuzzy logic-based direct torque control of three-phase induction motor," *Electrotechnical Review*, vol. 1, no. 2, pp. 102–105, Feb. 2023, doi: 10.15199/48.2023.02.16.
[22] K. K. Rout *et al.*, "Perturb and observe maximum power point tracking approach for microgrid linked photovoltaic system," *Indonesian Journal of Electrical Engineering and Computer Science*, vol. 29, no. 2, pp. 635–643, Feb. 2023, doi: 10.11591/ijeecs.v29.i2.pp635-643.
[23] R. Masmoudi, I. Boulhares, and A. Necaibia, "A new approach of variable step-size maximum power point tracking algorithm used in photovoltaic systems," *Indonesian Journal of Electrical Engineering and Computer Science*, vol. 28, no. 1, pp. 21–29, Oct. 2022, doi: 10.11591/ijeecs.v28.i1.pp21-29.
[24] K. Ishaque, Z. Salam, M. Amjad, and S. Mekhilef, "An improved particle swarm optimization (PSO)–based MPPT for PV with reduced steady-state oscillation," *IEEE Transactions on Power Electronics*, vol. 27, no. 8, pp. 3627–3638, Aug. 2012, doi: 10.1109/TPEL.2012.2185713.
[25] H. M. Abd Alhussain and N. Yasin, "Modeling and simulation of solar PV module for comparison of two MPPT algorithms (P&O and INC) in MATLAB/Simulink," *Indonesian Journal of Electrical Engineering and Computer Science*, vol. 18, no. 2, pp. 666–677, May 2020, doi: 10.11591/ijeecs.v18.i2.pp666-677.
[26] M. Irshaid and S. Abu-Eisheh, "Application of adaptive neuro-fuzzy inference system in modelling home-based trip generation," *Ain Shams Engineering Journal*, vol. 14, no. 11, p. 102523, Nov. 2023, doi: 10.1016/j.asej.2023.102523.
[27] P. Keikhosrokiani *et al.*, "Heartbeat sound classification using a hybrid adaptive neuro-fuzzy inference system (ANFIS) and artificial bee colony," *Digital Health*, vol. 9, Jan. 2023, doi: 10.1177/20552076221150741.
[28] M. Mokhtari *et al.*, "Voltage stability improvement of an asynchronous wind turbine using static var compensator with single-input fuzzy logic controller," in *Proc. 2018 6th Int. Renewable and Sustainable Energy Conference (IRSEC)*, Rabat, Morocco, Dec. 2018, pp. 1–6, doi: 10.1109/IRSEC.2018.8702872.
[29] B. Rachida *et al.*, "Implementation and analysis of adaptive neural fuzzy inference system-based brushless DC motor," in *Proc. 2023 3rd Int. Conf. Innovative Research in Applied Science, Engineering and Technology (IRASET)*, Mohammedia, Morocco, May 2023, pp. 1–6, doi: 10.1109/IRASET57153.2023.10152892.
[30] D. Fereka, "Performance improvement of ANFIS with sliding mode based on MRAS sensorless speed controller for induction motor drive," *Electrotechnical Review*, vol. 1, no. 12, pp. 271–277, Dec. 2019, doi: 10.15199/48.2019.12.61.

[31] J.-S. R. Jang and C.-T. Sun, "Neuro-fuzzy modeling and control," *Proceedings of the IEEE*, vol. 83, no. 3, pp. 378–406, Mar. 1995, doi: 10.1109/5.364486.
[32] A. Kusagur, S. F. Kodad, and B. V. S. Ram, "Modeling, design and simulation of an adaptive neuro-fuzzy inference system (ANFIS) for speed control of induction motor," *International Journal of Computer Applications*, vol. 6, no. 12, pp. 29–44, Sep. 2010, doi: 10.5120/1123-1472.
[33] S. Arslankaya, "Comparison of performances of fuzzy logic and adaptive neuro-fuzzy inference system (ANFIS) for estimating employee labor loss," *Journal of Engineering Research*, vol. 11, no. 4, pp. 469–477, Dec. 2023, doi: 10.1016/j.jer.2023.100107.
[34] M. N. M. Salleh, N. Talpur, and K. Hussain, "Adaptive neuro-fuzzy inference system: Overview, strengths, limitations, and solutions," in *Lecture Notes in Computer Science: Data Mining and Big Data*, vol. 10387, Springer, 2017, pp. 527–535, doi: 10.1007/978-3-319-61845-6_52.
[35] M. B. Nejad, S. M. Ghamari, and H. Mollaee, "Adaptive neuro-fuzzy inference systems controller design on Buck converter," *The Journal of Engineering*, vol. 2023, no. 10, p. e12316, Oct. 2023, doi: 10.1049/tje2.12316.
[36] X. C. Chen *et al.*, "Analysis and design of oil cooling structure in motor shaft of new energy vehicle," *Electrical Engineering and Automation*, vol. 69, no. 4, pp. 26–34, Nov. 2021, doi: 10.46904/eea.21.69.4.1108003.

BIOGRAPHIES OF AUTHORS

Laoufi Abdelhaq obtained his licence LMD degree in general electrotechnical engineering in 2012 from the university of abou bakr belkaid Tlemcen Algeria. In 2014 he obtained a Master's LMD degree in electrotechnical engineering option in machines control at the university of abou bakr belkaid in tlemcen algeria, since 2021 he is a doctoral student in Automatic control option of machines control Department of Electrical Engineering, Faculty of Sciences and Technology, University Mustapha Stambouli of Mascara, Algeria. He can be contacted at email: abdelhaq.laoufi@univ-mascara.dz.

Chergui Moulay-Idriss lecturer of Department of Electrical Engineering, University Mustapha Stambouli of Mascara. obtained diploma of deepened studies (DEA) in1993 PARIS-CNAM, magistère in electrotechnics in 1998 University of the USTO-MB Oran and in 2013 doctorate Es-sciences in Electrotechnics, University of the USTO-MB Oran. He can be contacted at email: chergui_cum@yahoo.fr.

Dr. Soufiane Chekroun Soufyane chekroun was born in Tlemcen, Algeria in 1983. He received his B.S from University of Sciences and Technology of Oran-Algeria in 2006 and M.S degrees from National School of Oran, ENP-Oran in 2009 and Ph.D. degrees in Automatic from University of Sciences and Technology of Oran-Algeria in 2016. Following graduation, he joined the department of Electrical Engineering of ENP-Oran as a research associate. Actually, he is associate Professor at University Mustapha Stambouli of Mascara-Algeria. His research interests include electrical machines, development of intelligent applications and the practical developments of high-performance electrical motor derive, and their related knowledge control schemes. He can be contacted at email: s.chekroun@univ-mascara.dz.